

# Keck Spectroscopy of distant GOODS Spheroidal Galaxies: Downsizing in a Hierarchical Universe

Tommaso Treu<sup>1,2</sup>, Richard S. Ellis<sup>2</sup>, Ting X. Liao<sup>2</sup>, Pieter G. van Dokkum<sup>3,2</sup>

## ABSTRACT

We analyze the evolution of the Fundamental Plane for 141 field spheroidal galaxies in the redshift range  $0.2 < z < 1.2$ , selected morphologically to a magnitude limit  $F850LP=22.43$  in the northern field of the Great Observatories Origin Survey. For massive galaxies we find that the bulk of the star formation was completed prior to  $z = 2$ . However, for the lower mass galaxies, the luminosity-weighted ages are significantly younger. The differential change in mass-to-light ratio correlates closely with rest-frame color, consistent with recent star formation and associated growth. Our data are consistent with *mass* rather than *environment* governing the overall growth, contrary to the expectations of hierarchical assembly. We discuss how feedback, conduction, and galaxy interactions may explain the downsizing trends seen within our large sample.

*Subject headings:* galaxies: elliptical and lenticular, cD — galaxies: evolution — galaxies: formation — galaxies: structure — cosmology: observations

## 1. Introduction

The question of the assembly history of elliptical and S0 (hereafter spheroidal) galaxies has come into sharp focus in recent years with the suggested discovery of their possible progenitors at redshifts above 2 (e.g., Chapman et al. 2003). However, the topic remains controversial both from a theoretical and observational standpoint.

---

<sup>1</sup>Department of Physics and Astronomy, University of California at Los Angeles, Los Angeles, CA 90095; ttreu@astro.ucla.edu; Hubble Fellow

<sup>2</sup>Caltech, Astronomy, 105-24, Pasadena, CA 91125, USA; rse@astro.caltech.edu, ting@caltech.edu

<sup>3</sup>Department of Astronomy, Yale University, New Haven, CT 06520; dokkum@astro.yale.edu

Semi-analytic models based on the current  $\Lambda$ CDM structure formation picture predict for spheroidals remarkably different assembly rates than observed (Benson et al. 2002), suggesting the effects of merging on stellar mass assembly are poorly understood. Consequently, the implication of recent claims for an abundant population of old massive systems at  $z \simeq 2$  are unclear (Glazebrook et al. 2004; Cimatti et al. 2004).

Exactly how the slow evolutionary trends observed in cluster spheroidals (Kelson et al. 1997; Bender et al. 1998; Stanford, Eisenhardt & Dickinson 1998; van Dokkum & Stanford 2003) contrast with those measured in the field (Treu et al 1999, 2001b, 2002; van Dokkum & Ellis 2003; Gebhardt et al. 2003; Rusin et al. 2003; Bernardi et al. 2003; Yi et al. 2005; Jimenez et al. 2004) is also unclear. The environmental dependencies do not appear to be as large (van Dokkum et al. 2001) as predicted by some renditions of hierarchical models (e.g. Diaferio et al. 2001; de Lucia et al. 2004). And those trends indicative of early assembly appear to be strongly at variance with the rapid decline in the red luminosity density claimed from large photometric samples (Bell et al 2004).

In this Letter we present the first results from a comprehensive Keck survey of 141 field spheroidals selected in the northern Great Observatories Origins Survey (GOODS) field. The spectroscopic signal to noise enables us to measure accurate stellar velocity dispersions for each spheroidal and, utilizing the Fundamental Plane (FP, Djorgovski & Davis 1987; Dressler et al. 1987), the dynamical mass and mass-to-light ratio. As these masses are closely linked to those of the underlying halos (Treu & Koopmans 2004), we establish a more complete picture of the assembly history than from studies based solely on photometrically-derived stellar masses. Our sample achieves a high degree of statistical completeness and is almost an order of magnitude larger than any previous equivalent study. This enables us to examine the rate of assembly as a function of dynamical mass and environmental density, both key variables for testing the currently-popular hierarchical picture for galaxy formation.

We assume throughout a cosmological model with  $\Omega_M = 0.3$ ,  $\Omega_\Lambda = 0.7$  and  $H_0 = 65$  km s<sup>-1</sup> Mpc<sup>-1</sup>. All magnitudes are in the AB system (Oke 1974), unless otherwise noted.

## 2. Data

In order to compare properly with local E+S0 galaxies, our parent sample was selected morphologically using visual classification to a F850LP magnitude limit of 22.43 (AB). Internal tests (Treu et al. 2005, in preparation, hereafter T05) show that our classification is self-consistent. The surface density of spheroidals is in agreement with that found by comparable studies (e.g.  $1.32 \pm 0.09$  arcmin<sup>-2</sup> vs.  $1.23 \pm 0.10$  arcmin<sup>-2</sup> measured by Im et al. 2002

to the same depth), showing that our classification is consistent with previous work and that the surface density is comparable with that expected from the local luminosity function.

High signal-to-noise spectra were obtained during April 1-5 2003 using the DEIMOS spectrograph at the Keck-II Telescope. Conditions were excellent with seeing in the range 0''.6-0''.8 throughout. The 1200 grating blazed at 7500Å was centered at 8000 Å. Total exposure times ranged between 14,400 and 38,900 seconds. The DEIMOS spectra were reduced using the IDL pipeline developed for the DEEP2 Survey (Davis et al 2003).

Stellar velocity dispersion were derived for 141 spheroidals (out of 163 spectroscopically targeted) using the methods described in Treu et al. (1999,2001a). To estimate systematic errors, a subsample was analyzed independently using methods described in van Dokkum & Franx (1996). The independent determinations agree within 1% on average (12% rms), indicating that systematic differences due to methodology are negligible. Comparisons with previously-published dispersions in the Hubble Deep Field (van Dokkum & Ellis 2003) as well as repeat DEIMOS measures for targets on different masks show that our estimated errors ( $\sim 10\%$ ) are reliable. Surface photometry through  $r^{1/4}$  model fitting was derived from the images using the GALFIT package (Peng et al. 2002).

A comparison of the subsample with measured velocity dispersions with the parent sample of morphologically selected spheroidals shows it to be representative with respect to color, luminosity and redshift distribution. We conclude that our sample is representative of morphologically selected spheroidals. The catalog, a description of the sample, related selection effects, observations and data reduction are given in T05.

In order to test for environmental trends, local projected densities were derived for individual spheroidals using a modification of the algorithm described in Dressler (1980) and the GOODS-N photometric catalog of Bundy, Ellis & Conselice (2004; hereafter B04). The B04 catalog includes spectroscopic redshifts from this survey and the Keck Team Redshift Survey (Wirth et al. 2004), with relatively uniform spatial sampling, supplemented by photometric redshifts (for the remaining 45% of the objects). For each spheroidal, we identify nearby objects brighter than  $M_V = -19.8$ , allowing for passive evolution. Then, moving away on the plane of the sky, we add the probability that each neighbor lies within  $3000 \text{ km s}^{-1}$  until a total number 5 is reached. This defines the local density  $\Sigma_5$ . We chose 5 nearest neighbors (rather than the usual 10) to enhance sensitivity to more modest overdensities, resulting in a poisson noise component of  $\sim 0.2$  dex. The partial use of photo-z brings the total error on  $\Sigma_5$  to 0.3 dex per galaxy (as calculated with simulations) .

### 3. Results

#### 3.1. Evolution of the Fundamental Plane

The Fundamental Plane (FP) is defined as:

$$\log R_e = \alpha \log \sigma + \beta \text{SB}_e + \gamma. \quad (1)$$

where  $R_e$  and  $\text{SB}_e$  are the effective radius and surface brightness and  $\sigma$  is the central velocity dispersion. A physical interpretation of the evolution of the FP follows from defining an effective (dynamical) mass,

$$M \equiv \frac{5\sigma^2 R_e}{G}. \quad (2)$$

Redshift variations of the slopes  $\alpha$ ,  $\beta$  and intercept  $\gamma$  can be interpreted via evolution of the stellar populations. If  $\sigma$  and  $R_e$  and Eq. 2 do not evolve, for the  $i$ th galaxy:

$$\gamma^i \equiv \log R_e^i - \alpha \log \sigma^i - \beta \text{SB}_e^i, \quad (3)$$

and the offset from the FP ( $\Delta\gamma^i \equiv \gamma^i - \gamma$ ) is related to the offset of the  $M/L$  by

$$\Delta \log \left( \frac{M}{L} \right)^i = -\frac{\Delta\gamma^i}{2.5\beta}. \quad (4)$$

The scatter of the FP ( $\sim 0.1$  in  $\log R_e$ ; Bernardi et al. 2003) is thus a measure of the homogeneity of the stellar population (see Treu et al. 2001b for more discussion).

Figure 1 shows the offset from the relation for the local Coma Cluster<sup>1</sup> using Eq. 4 for all 141 GOODS-N spheroids coded by dynamical mass (Eq 2). Evolutionary tracks for single burst stellar populations (Treu et al. 2001b) at various formation redshift ( $z_f = 1, 2, 5$ ) are shown for comparison. The most massive spheroidals uniformly follow a passive evolutionary trend consistent with an early epoch of formation, as found for massive cluster galaxies (e.g. van Dokkum & Stanford 2003). However, those with smaller masses are systematically younger (as hinted previously by smaller samples; Treu et al. 2002, van der Wel et al. 2004) and show increased scatter, implying a lower redshift of formation or secondary episodes of activity which rejuvenated a previously old population (e.g. Trager et al. 2000; Treu et al. 2002; van Dokkum & Ellis 2003).

We can verify that recent star formation is responsible for the trends in Figure 1 by comparing  $M/L$  with independent diagnostics of recent stellar formation, such as the rest-frame color (Figure 2). If we assume that the stellar  $M_*/L_B$  can be obtained as  $\Delta \log M/L_B$

---

<sup>1</sup>We use Coma as the local reference for both cluster and field to minimize systematic uncertainties related to filter transformations, distance determination and selection effects; see discussion in Treu et al. 2001b.

+  $\log M_*/L_{B,z=0}$  with  $M_*/L_{B,z=0} = 7.3M_\odot/L_{B,\odot}$  (Treu & Koopmans 2004), we can reproduce the locus for an ageing single burst population with a Salpeter IMF (red line in Figure 1). The observed correlation is fairly close to this model, although the scatter is significant, presumably as a result of a mixture of primary and secondary episodes of star formation, and, possibly, of metallicities. The analysis of spectral diagnostics such as Balmer absorption lines (T05) is also consistent with the trend in  $M/L$  being due to recent starformation.

### 3.2. The role of mass and environment

Our large and homogeneous sample allows us to take a significant step forward with respect to previous studies by exploring further the trends of  $M/L$  with dynamical mass introduced in §3.1 and by examining the correlations between  $M/L$  and local galaxy density,  $\Sigma_5$ . Dynamical mass can be an effective proxy for the total halo mass (Treu & Koopmans 2004) and local density (§ 2) for environmental effects. Therefore, we can use these correlations to study the role of halo mass and environment in the context of contemporary models of structure formation. To this aim, we will consider the quantity  $\delta\Delta \log M/L_B$ , defined as the difference between  $\Delta \log M/L_B$  for an individual spheroidal and that expected for old massive cluster galaxies at that redshift (i.e.  $\Delta \log M/L_B = -0.46z$ , van Dokkum & Stanford 2003). Negative values of  $\delta\Delta \log M/L_B$  indicate a smaller  $M/L_B$  than that of a massive cluster spheroid.

Figure 3 shows  $\delta\Delta \log M/L_B$  as a function of galaxy mass; a clear trend is evident with lower mass galaxies displaying younger luminosity-weighted ages. Although the two axes are not independent (a larger mass implies a larger  $M/L$  neglecting errors on  $L_B$ ), both the small error bars (typically  $< 0.1$  dex) and correlation with independent diagnostics (Figure 2; T05) indicate this trend does not arise from correlated uncertainties. Because of age and luminosity limits, a parent mass-selected sample must generally occupy a triangular region between the horizontal blue line and the lowest observed  $\delta\Delta \log M/L_B$  at any given mass. We thus conclude that the luminosity-weighted age of spheroidals increases with dynamical mass, a result we statistically confirm using detailed Monte Carlo simulations in T05.

We illustrate the effects of secondary bursts of star formation in Figure 3 by considering a family of two burst models, arranged by adding a young stellar component (aged 1 Gyr) to an earlier population (10 Gyr) equal for simplicity to the dynamical mass. For example a secondary burst of  $10^9$ - $10^{10}M_\odot$  would reproduce the observed trend.

Figure 4 shows  $\delta\Delta \log M/L_B$  as a function of local density  $\Sigma_5$ . No statistically significant correlation is present, although the dynamic range in GOODS-N does not include massive

clusters. Within our larger error bars, our data are consistent with the trend observed locally in the Sloan Digital Sky Survey (SDSS; Bernardi et al. 2003), which in turn can be explained in terms of mass differences in the context of environment-dependent mass functions. More pronounced is the difference with massive galaxies in the cores of rich clusters ( $\delta\Delta \log M/L_B \equiv 0$ ), although the poor statistics available for clusters at comparable redshifts and the different selection criteria prevent a detailed comparison.

#### 4. Discussion

We have shown that mass is a key variable determining the star formation history of field spheroidals. The most massive examples ( $> 10^{11.5} M_\odot$ ) formed most of their stars before  $z \simeq 2$ , while less massive ones ( $< 10^{11} M_\odot$ ) show greater scatter and systematically younger stellar ages. The secondary activity necessary to reproduce our observations (up to  $\sim 10^{10} M_\odot$  over the past few Gyr) could be explained by accretion of satellites or gas-rich mergers. Regardless of the process, substantial recent growth is implied in many cases for galaxies less massive than  $10^{11} M_\odot$ .

Such “downsizing” (i.e. stellar growth that moves systematically to lower mass systems as the Universe expands; Cowie et al. 1996) appears contrary to the expectations of hierarchical models of galaxy formation (Diaferio et al. 2001). In this widely-discussed picture, massive spheroidals assembled recently via major mergers with associated star formation. Strong environmental trends are also expected in such a picture (e.g. De Lucia et al. 2004), as a result of the fact that evolution is accelerated in these “biased” regions. We do not find any environmental trend within the range of densities covered by the GOODS-N field, although a larger sample of data will be needed to confirm this and properly compare with dense clusters, by studying the bivariate distribution (mass and local density) of  $\delta\Delta \log M/L_B$ .

Our observations may be reconciled with the hierarchical paradigm via the introduction of more detailed physics that regulates star formation in collapsing systems. If, above a certain halo mass, feedback from Supernovae or AGN, or thermal conduction (Benson et al. 2003; Nagashima et al. 2004; Granato et al. 2004), heat or remove gas and prevent it from cooling back onto the galaxy – thus inhibiting star formation – then the most massive galaxies will appear old even if they assembled dynamically at recent times, e.g. via collisionless mergers. Alternatively, star formation could be anticipated in massive system, triggered by galaxy interactions (Menci et al. 2004). Although infalling satellites or minor mergers may be frequent, they are likely to influence only the lower mass systems, as observed. The extended timescale necessary for lower mass mergers to relax and present smooth morphological systems may also play a key role (Hernandez & Lee 2004). Regardless of the detailed

explanation, it is clear that the mass-dependent growth of spheroidals is more complex than previously thought. It will be interesting to see if the numerical models with these additional mechanisms can reproduce quantitatively our result.

We acknowledge the use of the Gauss-Hermite Pixel Fitting Software developed by R. P. van der Marel and financial support by NASA (Hubble Fellowship HF-01167.01; STScI-AR-09960) and NSF (AST-0307859). We thank those who developed DEIMOS, the staff of the Keck Observatory, and the DEEP2 team for encouragement and assistance with observations and data reduction. We acknowledge discussions with A. Benson, B. Abraham, G. Bertin, R. Carlberg, K. Glazebrook, X. Hernandez, M. Malkan, A. Renzini, S. White. Based on data obtained with the HST operated by AURA for NASA and with the W.M. Keck Observatory on Mauna Kea, Hawaii, operated by Caltech, UC, and NASA and made possible by the W.M. Keck Foundation. We thank the referee for constructive criticism.

## REFERENCES

- Bell, E. et al. 2004, *ApJ*, 608, 752
- Bernardi M., et al. 2003, *AJ*, 125, 1866
- Bender, R., Saglia, R. P., Ziegler, B., Belloni, P., Greggio, L., Hopp, U., Bruzual, G., 1998, *ApJ*, 493,
- Benson, A.J., Ellis, R.S. & Menanteau, F. 2002, *MNRAS*, 336, 564
- Benson, A.J., Bower, R.G., Frenk, C.S., Lacey, C.G., Baugh, C.M., Cole, S. 2003, *ApJ*, 599, 38
- Bundy, K., Ellis, R.S., & Conselice, C.J. 2004, *ApJ*, submitted
- Chapman, S.C., Smail, I., Blain, A.W., Ivinson, R.J. 2004, *ApJ*, 614, 671
- Cowie L.L., Songaila, A., Hu, E.M., Cohen J.G. 1996, *AJ*, 112, 839
- Cimatti, A. et al., 2004, *Nature*, 430, 184
- Davis, M. et al. 2003, *SPIE*, 4834, 161
- De Lucia, G., Kauffmann, G., & White, S.D.M. 2004, *MNRAS*, 349, 1101

- Diaferio, A., Kauffmann, G., Balogh, M.L., White, S.D.M., Schade, D., Ellingson, E. 2001, MNRAS, 323, 999
- Djorgovski S. G., Davis M., 1987, ApJ, 313, 59
- Dressler, A. 1980, ApJ, 236, 351
- Dressler, A., Lynden-Bell, D., Burstein, D., Davies, R. L., Faber, S. M., Terlevich, R, Wegner G. 1987, ApJ, 313, 42
- Glazebrook, K. et al. 2004, Nature, 430, 181
- Gebhardt, K. et al. 2003, ApJ, 597, 239
- Granato, G.L., De Zotti, G., Silva, L., Bressan, A., Danese, L. 2004, ApJ, 600, 580
- Hernandez, X. & Lee, W.H., 2004, MNRAS, 347, 1304
- Jimenez, R. Panther, B., Heavens, A., & Verde, L. 2004, MNRAS, in press
- Kelson, D. D., van Dokkum, P. G., Franx, M., Illingworth G. D., & Fabricant, D. G. M. 1997, ApJ, 478, L13
- Menci, N., Cavaliere, A., Fontana, A., Giallongo, E., Poli, F. & Vittorini, V. 2004, ApJ, 604, 12
- Nagashima, M., Lacey, C., Baugh, C.M., Frenk, C.S., Cole, S. 2004, MNRAS, in press
- Peng, C., Ho, L.C., Impey, C.D., Rix, H.-W. 2002, AJ, 124, 266
- Rusin, D. et al. 2003, ApJ, 587, 143
- Stanford, S.A., Eisenhardt, P.R., Dickinson, M.E., 1998, ApJ, 492, 461
- Trager S. C., Faber S. M., Worthey G., Gonzalez J. J., 2000, AJ, 119, 1645
- Treu, T. & Koopmans, L. V. E. 2004, ApJ, 611, 739
- Treu, T., Stiavelli, M., Casertano, C., Møller, P., & Bertin G. 1999, MNRAS, 308, 1307
- Treu, T., Stiavelli, M., Møller, P., Casertano, C., & Bertin G. 2001a, MNRAS, 326, 221
- Treu, T., Stiavelli, M., Bertin G., Casertano, C., & Møller, P. 2001b, MNRAS, 326, 237
- Treu, T., Stiavelli, M., Casertano, C., Møller, P., Bertin, G. 2002, ApJ, 564, L13



- van der Wel, A., Franx, M., van Dokkum, P.G. & Rix, H.-W. 2004, ApJ, 601, L5
- van Dokkum P., Franx M., 1996, MNRAS, 281, 985
- van Dokkum, P.G. & Ellis, R.S. 2003,
- van Dokkum, P.G., Stanford, S.A. 2003,
- van Dokkum, P. G., Franx, M., Kelson D. D. & Illingworth, G. D., 2001, ApJ, 553, L39
- Yi, S. et al. 2005, ApJ, 619, L111
- Wirth, G. et al. 2004, AJ, 127, 3121

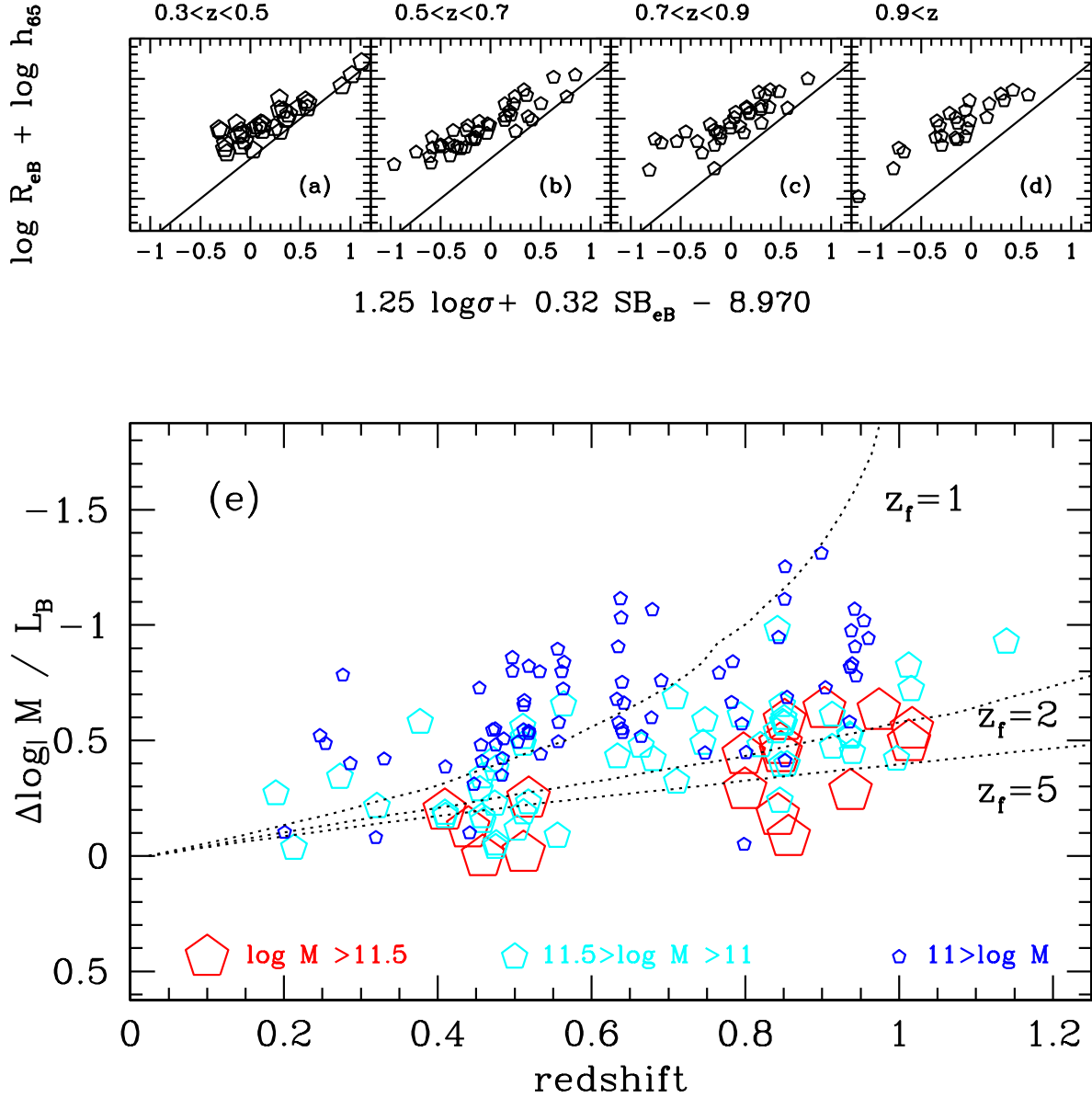


Fig. 1.— Top panels: edge-on view of the FP in redshift bins. The solid line represents the FP for the Coma cluster. Bottom panel: offset from the Coma FP, coded by dynamical mass demonstrating the stronger evolution for smaller masses. Typical errors are  $< 0.1$  dex on the vertical axis. Dotted lines represent passive evolutionary trends for single burst models at various formation epochs ( $z_f$ ).

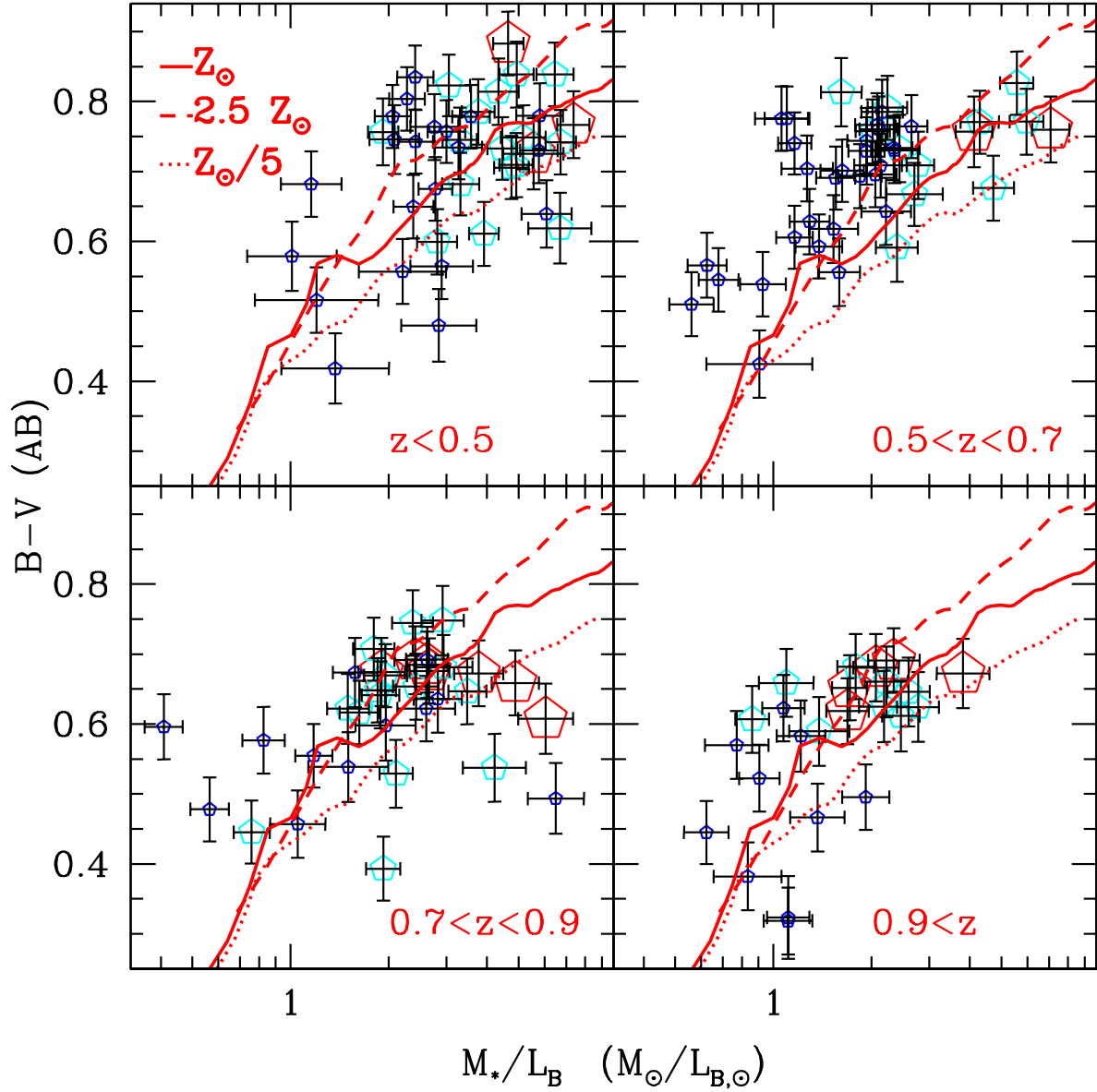


Fig. 2.— Rest frame (B-V) color as a function of the stellar mass to light ratio, obtained assuming a local value of  $7.3 M_{\odot}/L_{B,\odot}$ . The red curves are the tracks followed by single burst stellar populations with Salpeter IMF (ages 0.5 - 12 Gyrs) and various metallicities. The size of symbols represents galaxy mass as in Figure 1.

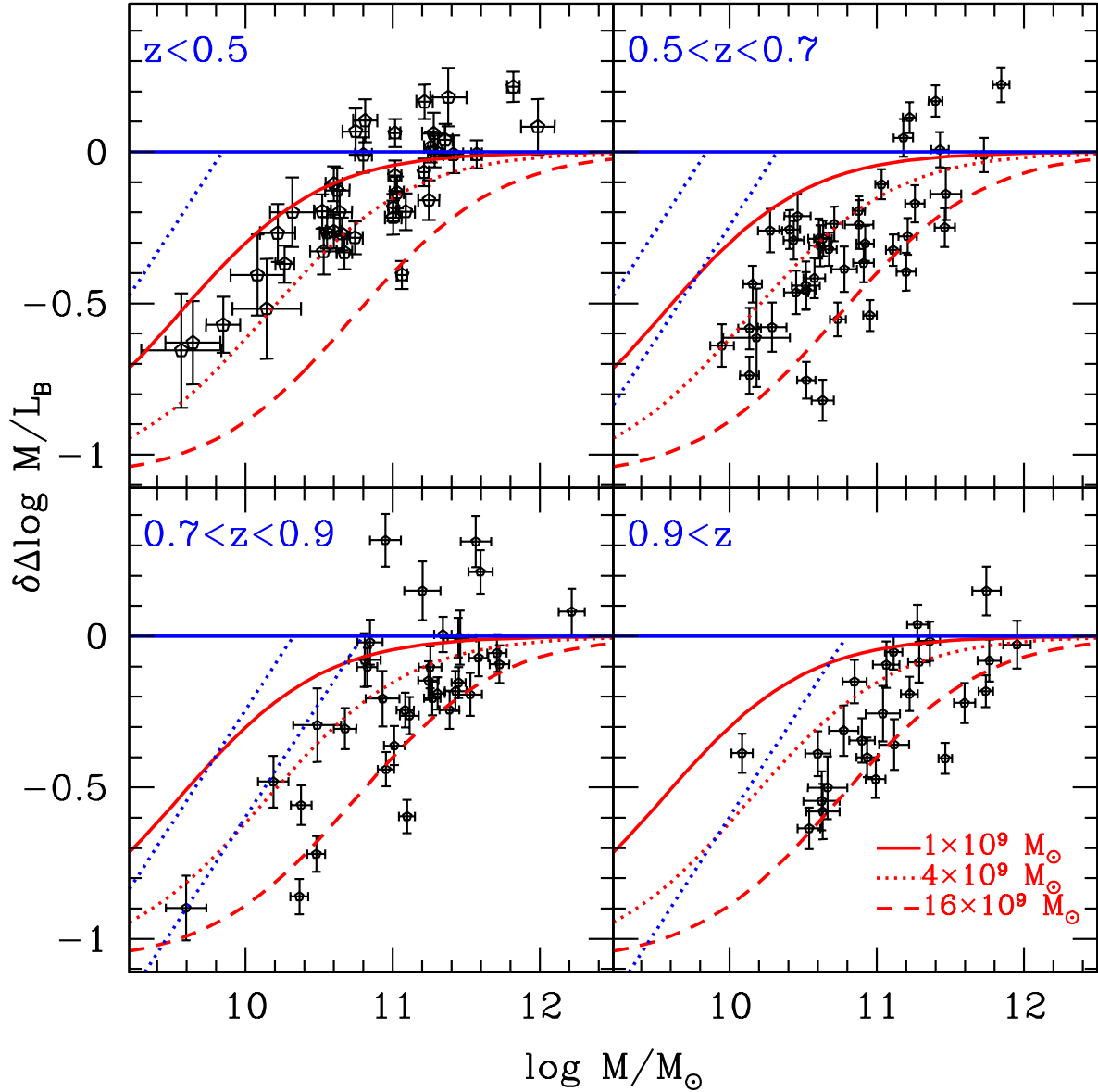


Fig. 3.—  $M/L_B$  offset with respect to the redshift-dependent behavior of old massive cluster spheroidals, plotted against dynamical mass  $M$ . The blue horizontal line represents the locus seen for massive cluster galaxies. Red curves illustrate the effects of secondary activity (1 Gyr ago) applied to a 10 Gyr old population of mass  $M$ . The blue (dotted) diagonal lines demonstrate the effect of the magnitude limit for each redshift bin.

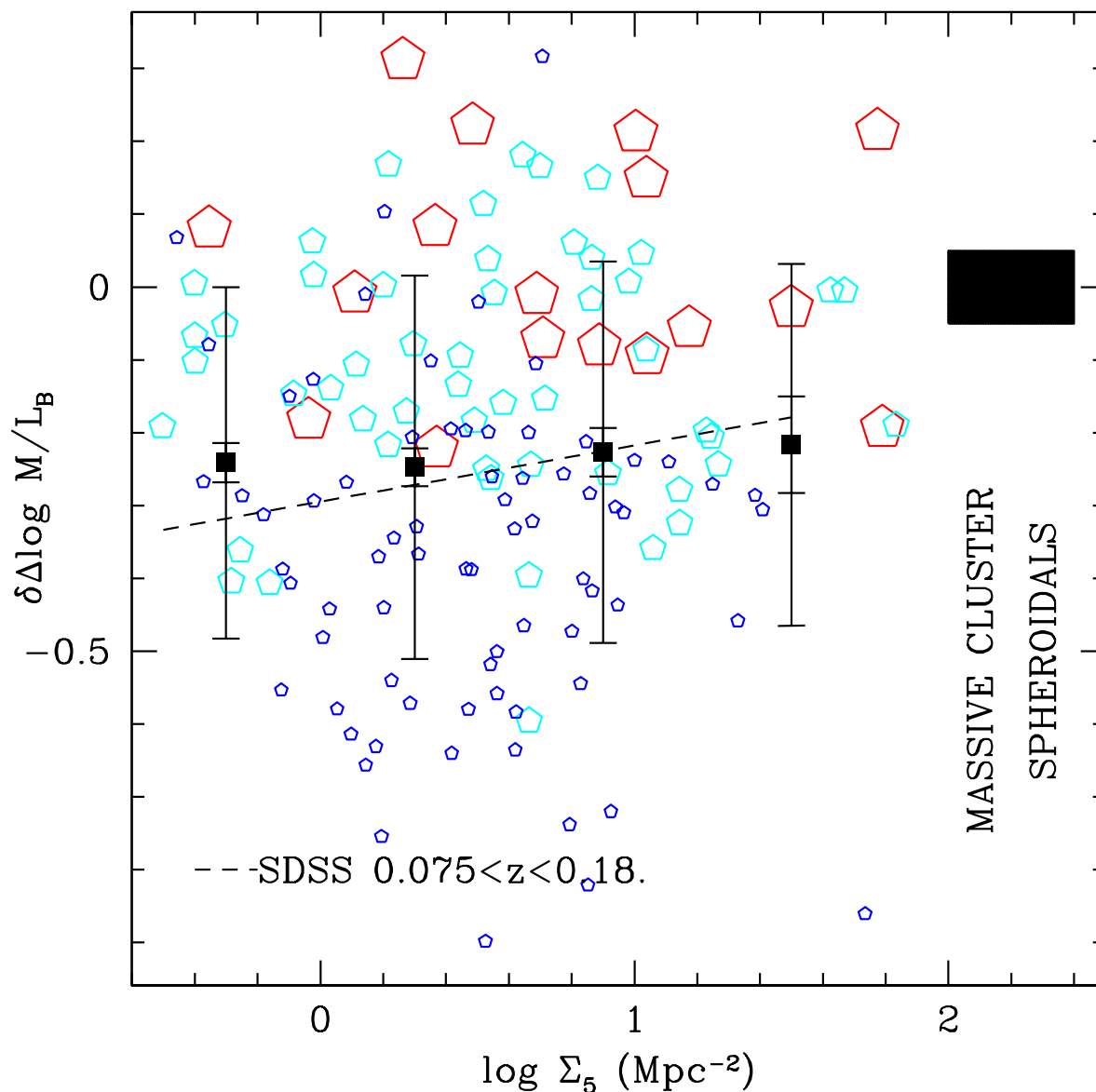


Fig. 4.— Offset of field spheroidals from the cluster trend ( $\delta\Delta M/L_B$ ) as a function of local projected density  $\Sigma_5$ , coded by mass as in Figure 1 (The error on the local density is  $\sim 0.3$  dex). Solid squares represent the averages in each density bin; large error bars represent the scatter, small error bars the uncertainty in the mean. The black rectangle represents the value observed for massive cluster spheroidals, the diagonal dashed line the local trend from the SDSS Survey (Bernardi et al. 2003).